Manuscript prepared for Earth Syst. Dynam.
with version 2015/04/24 7.83 Copernicus papers of the LATEX class copernicus.cls.
Date: 21 June 2017

On determining the Point of no Return in Climate Change

Brenda C. van Zalinge[1], Qing Yi Feng[1], Matthias Aengenheyster[1], and Henk A. Dijkstra[1]

[1]Institute for Marine and Atmospheric Research Utrecht, Department of Physics, Utrecht University, Utrecht, the Netherlands

Correspondence to: Qing Yi Feng (Q.Feng@uu.nl)

Abstract. Earth's global mean surface temperature has increased by about $1.0°C$ over the period 1880-2015. One of the main causes is thought to be the increase in atmospheric greenhouse gases. If greenhouse gas emissions are not substantially decreased, several studies indicate there will be a dangerous anthropogenic interference with climate by the end of this century. However, there is

5   no good quantitative measure to determine when it is 'too late' to start reducing greenhouse gas emissions in order to avoid such dangerous interference. In this study, we develop a method for determining a so-called 'point of no return' for several greenhouse gas emission scenarios. The method is based on a combination of aspects of stochastic viability theory and linear response theory, the latter being used to estimate the probability density function of the global mean surface temperature.

10 The innovative element in this approach is the applicability to high-dimensional climate models as is demonstrated by results obtained with the PlaSim model.

1   Introduction

In the year 2100, which is as far away (or as close) as 1932 in the past, mankind will be living on an Earth with a different climate than today. At that time, we will know the 2100-mean Global Mean

15 Surface Temperature (GMST) value and its increase, say ΔT, above the pre-industrial GMST value. From the then available GMST records, it will also be known whether this change in GMST has been gradual or whether it was rather 'bumpy'. If the observational effort will continue as of today, there will also be an adequate observational record to determine whether the probability of extreme events (e.g., flooding, heat waves) has increased.

20   The outcomes of these future observations, to be made by future generations, will strongly depend on socio-economic and technological developments and political decisions which are made now and over the next decades. Fortunately, there is a set of tools available to inform decision makers: Earth System Models. These models come in different flavours, from global climate models (GCMs) providing details on the development of the ocean-atmosphere-ice-land system to integrated assessment

25 models (AIMs) which also aim to describe the development of the broader socio-economic system.

During the preparation for the fifth assessment report (AR5) of the Intergovernmental Panel of Climate Change (IPCC), GCM studies have focussed on the climate system response to GHG changes as derived by AIMs from different socio-economic scenarios; the data from these simulations is gathered in the so-called CMIP5 archive (http://cmip-pcmdi.llnl.gov/cmip5/).

30   Depending on the representation of fast climate feedbacks in GCMs, determining their climate sensitivity, the CMIP5 models project a GMST increase ΔT of 2.5-4.5°C over the period 2000-2100 (Pachauri et al., 2014). This does not mean that the actual measured value of ΔT in 2100 will be in this interval. For example, the GMST may be well outside this range because of current model errors which misrepresented the strength of a specific feedback. As a consequence, a transition

35   might have occurred in the real climate system, which did not occur in any of the CMIP5 model simulations. Another possibility is that the GHG development eventually was far outside of the scenarios considered in CMIP5.

A crucial issue in 2100 will be whether a climate state has been reached where a dangerous anthropogenic interference (DAI) can be identified (Mann, 2009). In this case, present-day islands

40   will have been swallowed by the ocean, extreme events have increased in frequency and magnitude (Smith and Schneider, 2009). These effects are then very inhomogeneously distributed over the Earth and have lead to enormous socio-economic consequences. If this is the case in 2100, then there is a point in time where we must have crossed the conditions for DAI. This time, marking the boundary of a 'safe' and 'unsafe' climate state, obviously depends on the metrics used to quantify the state of

45   the complex climate system.

In very simplified views, this boundary is interpreted as a threshold on CO_2 concentration (Hansen et al., 2008) or on GMST. The latter, in particular the $\Delta T_c = 2°C$ threshold, has become an easy to communicate (and maybe therefore leading) idea to set mitigation targets for greenhouse gas reduction. Emission scenarios have been calculated (Rogelj et al., 2011) such that ΔT will remain

50   below ΔT_c. Although thresholds on GMST have been criticized for being very inadequate regarding impacts (Victor and Kennel, 2014), such a threshold forms the basis of policy making as is set forward in the Paris 2015 (COP21) agreement.

Suppose that measures are being taken to keep $\Delta T < \Delta T_c$, does this mean that we are 'safe'? The answer is a simple no, as regionally still DAI may have occurred such as the disappearance

55   of island chains due to sea level rise (Victor and Kennel, 2014). Hence, attempts have been made to define what 'safe' means in a more general way, such the Tolerable Windows Approach (TWA) (Petschel-Held et al., 1999) and Viability Theory (VT) (Aubin, 2009). These approaches also deal with general control strategies to steer a system towards 'safety' when needed. On a more abstract level, both TWA and VT start by defining a desirable (or 'safe') subspace V of a state vector $\mathbf{x}$ in a

60   general state space X. This subspace is characterized by constraints, such as thresholds on properties of $\mathbf{x}$. For example, when $\mathbf{x}$ is a high-dimensional state vector of a GCM, such a threshold could be $\Delta T < \Delta T_c$ on GMST. When the time-development (or trajectory) of $\mathbf{x}$ is such that it moves outside

the subspace V, a control is sought to steer the trajectory back into V. Note that this is an abstract formulation of the mitigation problem, when the amplitude of the emission of greenhouse gases is taken as control. Recently, Heitzig et al. (2016) have added more detail to regions in the space X which differ in their 'safety' properties and amount of flexibility in control to steer to 'safety'.

Given a certain desirable subspace of the climate system's state vector (e.g., to avoid DIA) and a suite of control options, (e.g., CO_2 emission reduction) it is important to know when it is too late to be able to steer the system to 'safe' conditions, say at the year 2100. In other words, when is the Point of No Return (PNR)? The TWA and VT approaches, and the theory in Heitzig et al. (2016), suffer from the 'curse of dimensionality' and cannot be used within CMIP5 climate models. For example, the optimization problems in VT and TWA lead to dynamic programming schemes which have up to now only been solved for model systems with low-dimensional state vectors. The approach in Heitzig et al. (2016) requires the computation of region boundaries in state space, which also becomes tedious in more than two dimensions. Hence, with these approaches it will be impossible to determine a PNR using reasonably detailed models of the climate system.

In this paper, we present an approach similar to TWA and VT, but one which can be applied to high-dimensional models of the climate system. Key in the approach is the estimation of the probability density function of the properties of the state vector $\mathbf{x}$ which determine the 'safe' subspace V. The PNR problem is coupled to limitations in the control options (e.g. of emissions) and can be defined precisely using these options and stochastic viability theory. The methodology is presented in section 2 and just to illustrate the concepts, we apply the approach in section 3 to an idealized energy balance model with and without tipping behavior. In section 4, the application to a high-dimensional climate model follows, using data from the Planet Simulator (PlaSim, Fraedrich et al. (2005)). A summary and discussion in section 5 concludes the paper.

2 Methodology

Here we briefly describe the concepts we need from stochastic viability theory and then define the PNR problem, specifically in the climate change context.

2.1 Viable states

Viability theory studies the control of the evolution of dynamical systems to stay within certain constraints on the system's state vector (Aubin, 2009). Here we consider finite dimensional deterministic systems, with state vector $\mathbf{x} \in R^d$ and vector field $\mathbf{f} : R^d \to R^d$, given by

$$\frac{d\mathbf{x}}{dt} = \mathbf{f}(\mathbf{x}, t). \tag{1}$$

In the general formulation of viability theory a time-dependent input is also considered in the right hand side of Eq. (1) which can be used to control the path of the trajectory $\mathbf{x}(t)$ in state space.

For our purposes, we only need the concept of a viable state, which is related to constraints on the state vector defining a viable region V in state space, also called the viability constraint set. In the model (1) such a set can, for example, be defined by a threshold condition $||\mathbf{x}|| < ||\mathbf{x}_*||$ An initial condition $\mathbf{x}_0 = \mathbf{x}(t = 0)$ is called viable if $\mathbf{x}(t) \in V$, for all $0 \leq t \leq t^*$, where t^* is a certain end time. The set of all these initial conditions forms the viability kernel associated with V.

Stochastic extensions of viability theory consider finite dynamical systems defined by stochastic differential equations

$$d\mathbf{X_t} = \mathbf{f}(\mathbf{X}_t, t)dt + \mathbf{g}(\mathbf{X}_t, t)d\mathbf{W}_t, \tag{2}$$

where $\mathbf{X}_t \in R^d$ is a multidimensional stochastic process, $\mathbf{W}_t \in R^n$ is a vector of n-independent standard Wiener processes and the matrix $\mathbf{g} \in R^{d \times n}$ describes the dependence of the noise on the state vector. The normalised probability density function (PDF) $p(\mathbf{x}, t)$ can be formally determined from the Fokker-Planck equation associated with Eq. (2).

A stochastic viability kernel V_β consists of initial conditions $\mathbf{X}_0$ for which the system has, for $0 \leq t \leq t^*$, a probability larger than a value β to stay in the viable region V (Doyen and De Lara, 2010). For example, in a one-dimensional version of Eq. (2) with state vector $X_t \in R$ and with a viable region V given by $x \leq x^*$ a state X_t is called viable, with tolerance probability β_T, if

$$\int\limits_{-\infty}^{x^*} p(x, t)\, dx \geq \beta_T, \tag{3}$$

and otherwise, X_t is called non viable.

2.2 Linear response theory

In relatively idealized low-dimensional models (such as the energy balance model in section 3), the probability density functions can be easily computed by solving for the Fokker-Planck equation (see section 3.2). However, in order to find the temporal evolution of the PDF of the global mean surface temperature GMST under any CO_2eq forcing in high-dimensional climate models, such as PlaSim in section 4, we will use linear response theory (LRT). With this theory, the effect of any small forcing perturbation on the system state can be calculated by running the climate model for only one forcing scenario (Ragone et al., 2014).

In LRT, the expectation value of an observable Φ, when forcing the system with a time-dependent function $f(t)$, can be calculated by computing the convolution of a Green's function $G_{\langle \Phi \rangle}$ and the forcing $f(t)$, according to

$$\langle \Phi \rangle_f(t) = \int\limits_{-\infty}^{+\infty} G_{\langle \Phi \rangle}(\tau) f(t - \tau) d\tau. \tag{4}$$

To construct this Green's function, the property that the convolution in the time domain is the same as point-wise multiplication in the frequency domain is used. The Fourier transform of Eq. (4) is

(a)   (b)
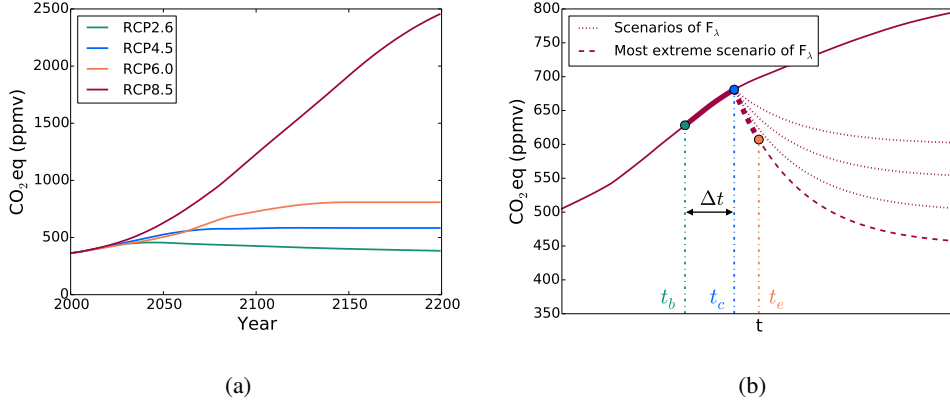
Figure 1. *(a) CO₂eq trajectories of the RCP scenarios used by the IPCC in CMIP5. (b) The solid red curve represents a typical RCP scenario. At the time t_b the climate state becomes non-viable, while at $t = t_c$ a CO₂eq reduction F_λ applies; at time t_e, the climate state is viable again.*

given by

$$\langle\widetilde{\Phi}\rangle_f(\omega) = \chi_{\langle\Phi\rangle}(\omega)\widetilde{f}(\omega), \tag{5}$$

130 with $\chi_{\langle\Phi\rangle}(\omega)$, $\langle\widetilde{\Phi}\rangle_f(\omega)$ and $\widetilde{f}(\omega)$ being the Fourier transforms of $G_{\langle\Phi\rangle}(t)$, $\langle\Phi\rangle_f(t)$ and $f(t)$, respectively. Therefore, once the time evolution of the expectation value of an observable under a certain forcing is known, the Green's function of this observable can be constructed with Eq. (5) and consequently the linear response of the observable to any forcing can be calculated.

2.3 The Point of No Return problem

135 In the climate change context, scenarios of GHG increase and the associated radiative forcing have been formulated as Representative Concentration Pathways (RCPs). In Pachauri et al. (2014), there are four RCP scenarios (Fig. 1a) ranging from an increase in radiative forcing of $2.6\,\mathrm{W\,m^{-2}}$ (RCP2.6) at 2100 (with respect to 2000) to a forcing increase of $8.5\,\mathrm{W\,m^{-2}}$ (RCP8.5).

To define the PNR for each of these RCPs, a collection of mitigation scenarios on greenhouse gas

140 emission has to be considered. These mitigation scenarios will lead to changes in GHG concentrations, described by functions $F_\lambda(t)$, where λ is a parameter. For instance, the collection F_λ could result from mitigation measures that lead to an exponential decay to different stabilisation levels (measured in CO₂ equivalent, or CO₂eq) within a certain time interval. An example of such a collection F_λ is shown by the dashed and dotted red lines in Fig. 1b. The most extreme member of F_λ

145 is defined as the mitigation scenario (represented by a certain value of parameter λ) which has the steepest initial decrease at a certain time t (dashed curve in Fig. 1b).

Along the curve of a certain RCP scenario, there will be a point in time where action will be taken to reduce emissions of GHG; this is indicated by a time of action t_b. Consider for example (Fig. 1b) that t_b is chosen as the first year where the state vector $\mathbf{X}_t$ is not viable anymore. A reduction in
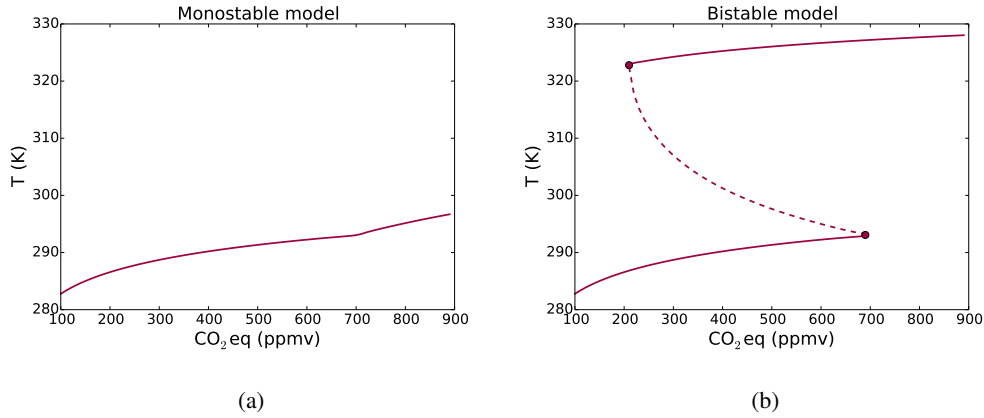
Figure 2. *Bifurcation diagram of the deterministic energy balance model for $\alpha_1 = 0.45$ ((a), monostable model) and $\alpha_1 = 0.2$ ((b), bistable model). The solid curve represents a stable equilibrium while a dashed curve represents an unstable equilibrium.*

emissions is, however, not immediately followed by a decrease in CO_2eq due to the long residence time of atmospheric CO_2. In addition, there is a delay to take action in emission reduction due to technological, social, economic and institutional challenges. Hence, emission reduction will only start Δt_1 years after t_b. The CO_2eq will, even after emissions have been reduced, also still increase over a time Δt_2. The time at which the CO_2eq starts to reduce according to F_λ is indicated by $t_c = t_b + \Delta t$, where $\Delta t = \Delta t_1 + \Delta t_2$. Eventually, $\mathbf{X}_t$ may become viable again and this point in time is indicated by t_e (Fig. 1b).

For a given RCP scenario, tolerance probability β_T, viable region V and collection F_λ, we define the PNR (π_t) as the first year t_c where, even when at that moment the most extreme CO_2eq reduction scenario F_λ applies,

(a) either $\mathbf{X}_t$ will be non viable for more than τ_T years, where τ_T is a set tolerance time, or

(b) $\mathbf{X}_t$ will be non viable in the year 2100.

The first PNR, which we will indicate below by π_t^{tol}, is based on limiting the amount of years that $\mathbf{X}_t$ is non viable, since (during these years) society is exposed to risks from, for example, extreme weather events. The second PNR, which we will indicate below by π_t^{2100} imposes no restrictions on how long $\mathbf{X}_t$ is non viable, but it is only based on that $\mathbf{X}_t$ is non viable at the end on this century. Hence, under the given set of mitigation options, it is guaranteed that the state will have left the viable region by the year 2100. We will use both PNR concepts in the results below.

3 Energy balance model

In this section, we illustrate the concepts and the computation of the PNR for an idealized energy balance model of Budyko-Seller type (Budyko, 1969; Sellers, 1969). We will also assume that the

CO_2eq can be directly controlled, and hence no carbon cycle model is needed to determine CO_2eq from an emission reduction scenario.

3.1 Formulation

We use the stochastic extension of the model formulation as in Hogg (2008). The equation for the atmospheric temperature T_t (in K) is given by

$$dT_t = \frac{1}{c_T}\left\{Q_0(1 - \alpha(T_t)) + G + A\ln\frac{C(t)}{C_{ref}} - \sigma\epsilon T_t^4\right\}dt + \sigma_s dW_t. \tag{6}$$

The values and meaning of the parameters in Eq. (6) are given in Table 1. The first term in the right hand side of Eq. (6) represents the short-wave radiation received by the surface and $\alpha(T)$ is the albedo function, given by

$$\alpha(T) = \alpha_0 H(T_0 - T) + \alpha_1 H(T - T_1) + \left(\alpha_0 + (\alpha_1 - \alpha_0)\frac{T - T_0}{T_1 - T_0}\right)H(T - T_0)H(T_1 - T). \tag{7}$$

This equation contains the effect of land ice on the albedo and $H(x) = 1/2(1 + \tanh(x/\epsilon_H))$ is a continuous approximation of the Heaviside function. When the temperature $T < T_0$, the albedo will be α_0 and when $T > T_1$ it will be α_1 and the albedo is linear in T for $T \in [T_0, T_1]$. The second term in the right hand side of Eq. (6) represents the effect of greenhouse gases on the temperature. It consists of a constant part (G), and a part ($A\ln\frac{C(t)}{C_0}$) depending on the mean CO_2eq concentration in the atmosphere (indicated by $C(t)$). The third term in the right hand side of Eq. (6) expresses the effect of long-wave radiation on the temperature and the last term represents noise with a constant standard deviation σ_s. The standard value of σ_s chosen as 3% of the value of G/c_T, hence about $0.3K$/year. The variance in CO_2 concentration originates mostly from seasonal variations, and the 3% is on the high side. Nevertheless, we still use this value, because if we take values smaller than 3% the PDF of the GMST will almost be a delta function and concepts can not be illustrated clearly.

3.2 Results: stochastic viability kernels

When using the global mean CO_2eq concentration C in Eq. (6) as a time-independent control parameter, a bifurcation diagram can be easily (numerically) calculated for the deterministic case ($\sigma_s = 0$). In Fig. 2, such diagrams are plotted of C versus the equilibrium temperature T for two values of α_1. To obtain realistic values for the temperature, the equilibrium temperature equilibria are shifted upwards by 30 K. This is done by substituting T with $T - 30$ and adapting the right hand side of Eq. (6) such that the new temperature is a steady state. This is obviously a bit artificial here, but we justify it by our aim to only wanting to illustrate the methodology; results from more realistic models will follow in section 4 below. The diagram corresponding to $\alpha_1 = 0.2$ (Fig. 2a) has two saddle-node bifurcations which are absent for $\alpha_1 = 0.45$ (Fig. 2b). From now on, the energy balance model with $\alpha_1 = 0.45$ and $\alpha_1 = 0.2$ will be called the monostable and bistable case, respectively.

Table 1. *Value and meaning of the parameters in the energy balance model given by Eq. (6).*

c_T	5.0×10^8 Jm^{-2}K^{-1}	Thermal inertia	ϵ	1.0	Emissivity
Q_0	342 Wm^{-2}	Solar constant/4	α_0	0.7	Albedo parameter
G	1.5×10^2 Wm^{-2}	Constant	α_1	0.2 or 0.45	Albedo parameter
A	2.05×10^1 Wm^{-2}	Constant	T_0	263 K	Albedo parameter
C_{ref}	280 ppmv	Reference CO_2 concentration	T_1	293 K	Albedo parameter
σ	5.67 x 10^{-8} Wm^{-2}K^{-4}	Stefan Boltzmann constant	ϵ_H	0.273 K	Albedo parameter

For $\sigma_s \neq 0$, we explicitly determine the normalised PDF $p(x,t)$. Rewriting Eq. (6) as

$$dT_t = f(T_t,t)dt + \sigma_s dW_t, \tag{8}$$

with $f(T,t) = c_T^{-1}(Q_0(1-\alpha(T)) + G + A\ln\frac{C(t)}{C_{ref}} - \sigma\epsilon T^4)$, the Fokker-Planck equation of Eq. (8) is given by

$$\frac{\partial p}{\partial t} + \frac{\partial(fp)}{\partial x} - \frac{\sigma_s^2}{2}\frac{\partial^2 p}{\partial x^2} = 0. \tag{9}$$

This differential equation is solved numerically for $p(x,t)$ under any prescribed function $C(t)$ with boundary conditions $p(x_u,t) = p(x_l,t) = 0$, where x_l = 270 K and x_u = 335 K, and an initial condition $p(x,0)$ (specified below) satisfying $\int_{x_l}^{x_u} p(x,0)dx = 1$.

We first show stochastic viability kernels for each initial condition T_0 and C_0, where C_0 is an initial CO$_2$eq concentration and T_0 is the expectation value of the initial PDF of T_t. As starting time, we take the year 2030 and suppose that the climate system will be forced by a certain RCP scenario from 2030 till 2200. For every C_0, the original RCP scenario from Fig. 1a is adjusted such that its time development remains the same, but it has C_0 as CO$_2$eq concentration in 2030. The PDF of the GMST $p(x,t=0)$ ($t=0$ refers to the year 2030) has a prescribed variance (defined by σ_s^2) and expectation value T_0.

In Fig. 3, the stochastic viability kernels are plotted for the energy balance model forced by the RCP4.5 scenario and a viable region V defined by $T \leq 293$ K. The results for the monostable and bistable cases are plotted in Fig. 3a and Fig. 3b, respectively. The colors indicate for each combination of T_0 and C_0 in which stochastic viability kernel the initial state (C_0, T_0) is located. For example, consider the bistable case and an initial condition of $T_0 = 288$ K and $C_0 = 400$ ppmv, then this initial condition is in the kernel V_β with $\beta \geq 0.9$. This means that, with a probability larger than 0.9, a trajectory of the model starting at (C_0, T_0) will remain viable up to the year 2200, where C follows the RCP4.5 scenario. The white areas contain initial conditions that are in a stochastic viability kernel V_β with $\beta < 0.5$.

The sensitivity of the stochastic viability kernels with respect to RCP scenario, threshold defining the viable region V and amplitude of the noise σ_s was also investigated (results not shown). The behaviour is as one can expect in that the area of the kernels becomes smaller (larger) when noise
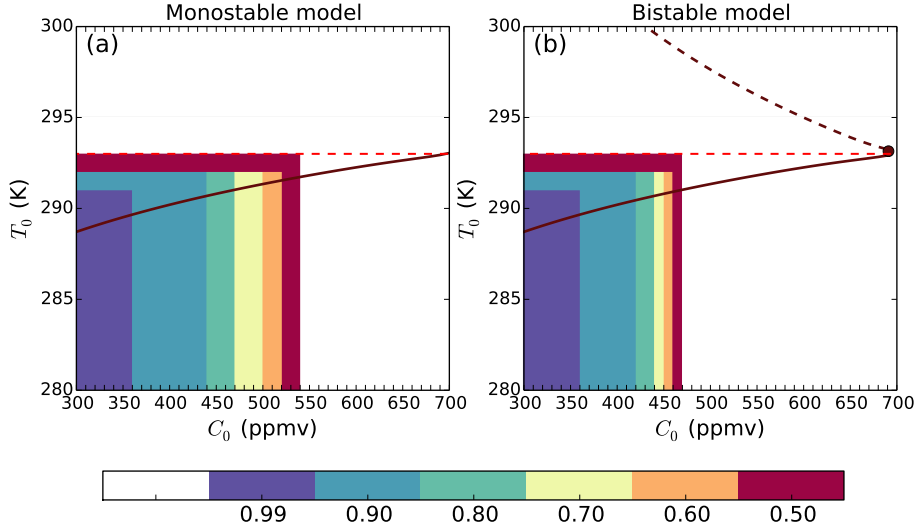
Figure 3. The stochastic viability kernels for the monostable and bistable cases forced by the RCP4.5 scenario. The viable region is defined as $T \leq 293K$ and is indicated by the red dashed line. This plots show, for each combination of T_0 and C_0, in which stochastic viability kernel these initial values are located. The numbers in the colourbar stand for the β in V_β. For convenience, the bifurcation diagram of the deterministic model is also shown.

230   is larger (smaller), when the threshold temperature is smaller (larger) and when the radiative forcing associated with the RCP scenario is more (less) severe. For example for the RCP6.0 scenario, each combination of T_0 and C_0 (same range as in Fig. 3) is in a V_β with $\beta < 0.5$ for both mono- and bistable cases.

3.3   Results: Point of No Return

235   Again for illustration purposes, we assume that reduction of the emissions will have an immediate effect of the CO_2eq, such that effectively the CO_2eq is controlled. We choose the collection F_λ to consist of mitigation scenarios that exponentially decay to the preindustrial CO_2eq concentration, which is 280 ppmv. For this exponential decay, we consider different e-folding times τ_d. The most extreme scenario has an exponential decay within 50 years, which corresponds to an e-folding time

240   of $\tau_d = 9$ years. Hence, the collection F_λ is given by (for $\tau_d \geq 9$)

$$F_\lambda(t) = (C_{t_c} - 280) \exp\left(-\frac{t - t_c}{\tau_d} \right) + 280. \tag{10}$$

In this equation, t_c is the time at which the scenario is applied and C_{t_c} the associated CO_2eq concentration at that moment.

Next, we determine PNR values π_t^{tol} for the energy balance model when it is forced by the four

245   different RCP scenarios using a tolerance probability of $\beta_T = 0.9$ and a tolerance time of $\tau_T = 20$

(a)
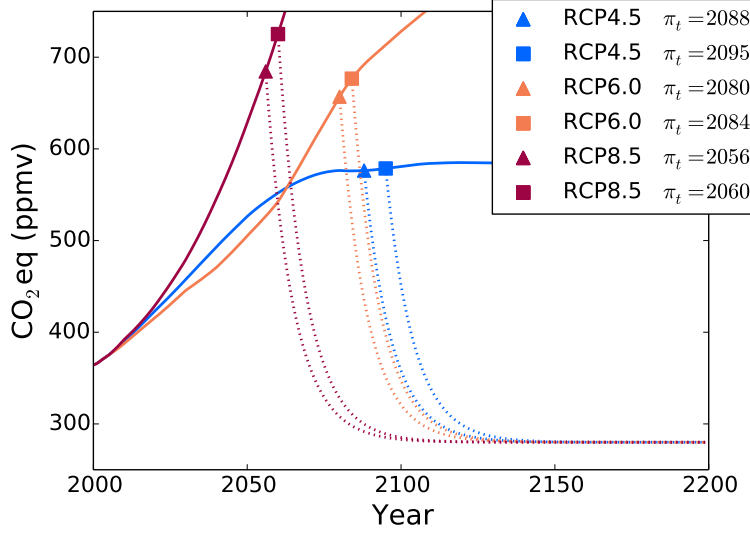
Figure 4. The PNR π_t^{tol} for a system forced with different RCP scenarios, tolerance probability $\beta_T = 0.9$ and tolerance time $\tau_T = t_e - t_b = 20$ years. The triangles indicate the point of no return for the bistable case and the squares for the monostable case. The dotted line is the most extreme scenario of F_λ with an exponential decay to 280 ppmv and an e-folding time of 9 years. Note that for both cases there is no PNR when the model is forced with the RCP2.6 scenario.

years. The π_t^{tol} values for a system forced with the RCP4.5, RCP6.0 and RCP8.5 scenarios are shown in Fig. 4 for both the monostable and bistable cases. As expected, the more extreme the RCP scenario, the earlier the PNR. This can be easily explained by the fact that when the CO_2eq concentration is rising faster, the temperature will get non viable earlier. Consequently, the PNR

250 will be earlier, since the GMST is only allowed to be non viable for at most τ_T years. When the model is forced with RCP2.6, there is no PNR for both models. The reason for this is that the CO_2eq concentration will remain low throughout the whole period and consequently the temperature will stay viable. The value of π_t^{tol} of the bistable case is for each scenario earlier than the value of the monostable case. This can be clarified by the fact that the PDF of the temperature in the bistable

255 case will leave the viable region at a lower CO_2eq concentration because of the existence of nearby equilibria.

The sensitivity of π_t^{tol} versus the tolerance time τ_T and the tolerance probability β_T was also investigated and the results are as expected (and therefore not shown). A longer tolerance time will shift π_t^{tol} to later times. For example, for the RCP4.5 scenario $\pi_t^{tol} = 2071,\ 2088$ and 2116 for

260 $\tau_T = 0, 20$ and 50 years for the bistable case (for fixed $\beta_T = 0.9$). With a fixed $\tau_T = 20$ years, the value of π_t^{tol} shifts to smaller values when the tolerance probability is increased. For example, for $\beta_T = 0.80$ and 0.99, the values of π_t^{tol} are 2127 and 2058, respectively, for the bistable case (for $\beta_T = 0.9$, $\pi_t^{tol} = 2088$, see Fig. 4).

4 PlaSim

265   The results in the previous section have illustrated that a PNR can be calculated when an estimate of the probability density function is available and a collection of mitigation scenarios is defined. We will now apply these concepts to the more detailed, high-dimensional, climate model PlaSim, a General Circulation Model developed by the University of Hamburg, see https://www.mi.uni-hamburg.de/en/arbeitsgruppen/theoretische-meteorologie/mod-

270   elle/plasim.html. The atmospheric dynamical processes are modelled using the primitive equations formulated for vorticity, divergence, temperature and the logarithm of surface pressure. Moisture is included by transport of water vapour (specific humidity). The governing equations are solved using the spectral transform method on a T21 grid (resulting in a horizontal resolution of about 5 to 6 degrees in the midlatitudes). In the vertical, 5 non-equally spaced sigma (pressure divided by surface

275   pressure) levels are used. Considering that the model has about a hundred prognostic variables, this yields an order of magnitude for the dimensionality of the model of about 10^5. The model is forced by diurnal and annual cycles. PlaSim is freely available including a graphical user interface facilitating its usage and has been applied to a variety of problems in climate response theory (Ragone et al., 2016).

280   A main problem here is to determine a relation between the CO_2eq (and associated radiative forcing) and the GMST, i.e. a response function. Previous approaches have used a fit of a specific response function (e.g., a power law function) to available observations (Rypdal, 2016). This is more complicated for an approach using stochastic viability theory (applying it did not give useful results) and hence we proceed by using linear response theory as described in section 2.3.

285   We use the same data as in Ragone et al. (2014), provided by F. Lunkeit and V. Lucarini (Univ. Hamburg, Germany). The difference with those in Ragone et al. (2014) is that the seasonal forcing is present, which results in a long-term increase of the GMST of 5 °C (instead of 8 °C in Ragone et al. (2014)) under a scenario where the CO_2 concentration doubles. The reason of this difference is not fully clear but probably results from seasonal rectification effects of nonlinear feedbacks. Data of

290   GMST from two ensembles was used, each of 200 simulations, made with two different CO_2 forcing profiles (all other GHGs are kept constant). For both forcing profiles, the starting CO_2 concentration is set to a value of 360 ppmv, which is representative for the CO_2 concentration in 2000. During the first set of experiments, the CO_2 concentration is instantaneously doubled to 720 ppmv and kept constant afterwards. During the second set of experiments, the CO_2 concentration increases each

295   year by 1 % until a concentration of 720 ppmv is reached. This will take approximately 70 years and afterwards the concentration is fixed. The total length of the simulations is 200 years. Furthermore, the forcing $f(t)$ in Eq. (4) is taken as the logarithm of the CO_2 concentration, since the radiative forcing scales approximately logarithmically with the CO_2 concentration.

    To determine the PDF of GMST under any CO_2eq forcing, we make the assumption that at each

300   point in time the PDF of the GMST is normally distributed. As we have 200 data points for the GMST
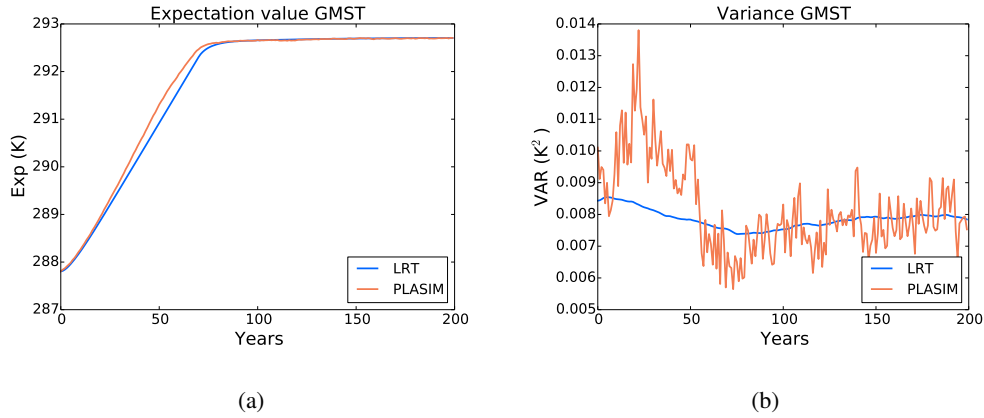
Figure 5. *(a) The expectation value and (b) variance of GMST generated by PlaSim (orange) and determined through LRT (blue) for the 1% CO_2 concentration increase.*

at each time interval, a χ^2 test was used to analyse the PDFs. For each time, the value of $\chi^2 > 0.05$ and therefore the assumption that the PDF of the GMST is normally distributed appears justified. The Green's functions for the expectation value and variance of GMST have been calculated with the instantaneously doubling CO_2 profile and the associated ensemble. From the ensemble, at each point in time the expectation value and variance are calculated to obtain the temporal evolution of these two variables. Subsequently, we have found the Green's functions using (5). To check whether these Green's functions perform well, we compared the temporal evolution of the expectation value and variance of the GMST under the 1 % forcing (calculated with (4)) with those directly generated with PlaSim (Fig. 5). The expectation value determined with LRT is close to the one directly generated by PlaSim. However, the variance of the ensemble generated by PlaSim is a lot noisier than the one calculated with LRT. Although the Green's function of the variance provides only a rough approximation, it has the right order of magnitude and we will use it to calculate the variance of the GMST for other forcing scenarios.

4.1 Results: Point of No Return under CO_2eq control

We first consider the case without a carbon cycle model, again assuming that the CO_2eq concentration can be controlled directly. The scenarios F_λ chosen for use in PlaSim are exponentially decaying to different stabilisation levels (varying between 400 and 550 ppmv, see Edenhofer et al. (2010)). This stabilization level is taken as the parameter λ. We assume that stabilisation happens within 100 years, which corresponds to an e-folding time τ_d of about 25 years; the mitigation scenarios F_λ are then given by

$$F_\lambda(t) = \left(C_{t_c} - \lambda\right) \exp\left(-\frac{t - t_c}{\tau_d}\right) + \lambda, \tag{11}$$

(a)   (b)
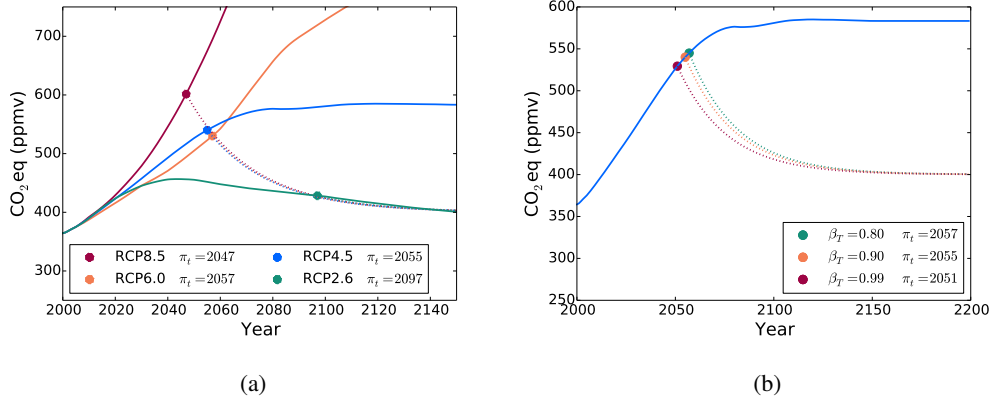
Figure 6. *(a) The PNR π_t^{2100} for the RCP2.6, RCP4.5, RCP6.0 and RCP8.5 scenarios for a tolerance probabil-ity of $\beta_T = 0.9$ and $\Delta t = 0$. The solid lines represent the RCP scenarios and the dashed line the most extreme scenario from F_λ. Note that these dashed lines coincide. (b) The point of no return for RCP4.5 for different tolerance probabilities.*

where t_c is again the time at which the mitigation scenario is applied and C_{t_c} the associated CO_2eq concentration. The most extreme mitigation scenario in F_λ in terms of CO_2eq decrease is the one that stabilises at a CO_2eq concentration of 400 ppmv.

325   We next determine the PNR π_t^{2100} by requiring that the GMST must be viable in 2100 using a tolerance probability of $\beta_T = 0.90$. Furthermore, the viable region is set at $T \leq 16.15°C$, which corresponds to temperatures less than 2°C above the preindustrial GMST. The values of π_t^{2100} for all the RCP scenarios are plotted in Fig. 6a. Solid curves show the RCP scenarios while dashed curves present the most extreme scenario F_λ. For RCP8.5, π_t^{2100} is 10 years earlier than for RCP6.0, since

330   the CO_2eq concentration increases much faster for the RCP8.5 scenario. The mitigation scenario after the point of no return, represented by the dashed line, is the same for all RCP scenarios. This is related to our definition of π_t^{2100}, where it is required that the GMST is viable in 2100. The mitigation scenario that is plotted is the ultimate scenario that guarantees this. It indicates that for each CO_2 scenario the associated π_t^{2100} is given by the intersection of that CO_2eq scenario and

335   the mitigation scenario. This is because it is considered that an exponential decay to 400 ppmv within 100 years is always possible, no matter the CO_2eq concentration at t_c. However, when this concentration becomes too high, this mitigation scenario is not very realistic anymore.

The influence of the tolerance probability on π_t^{2100} for the RCP4.5 scenario is plotted in Fig. 6b, where we only consider a tolerance probability of 0.8, 0.9 and 0.99. When the tolerance probability is

340   higher, it takes longer before the GMST will be viable again and thus the PNR π_t^{2100} will be earlier. However, the differences are very small, since the mitigation scenarios that guarantee viability in 2100 for the different tolerance probabilities are very close.

4.2 Results: Point of No Return under emission control

Finally, we consider the more realistic case where emissions are controlled and a carbon model converts emissions to CO_2eq. A simple carbon model relating emissions E to concentrations C is given by

$$C_{CO2}(t) = C_{CO2,0} + \int_0^t G_{CO2}(\tau)\, E_{CO2}(t-\tau)\, d\tau, \qquad (12)$$

where $C_{CO2,0}$ is the initial concentration. The Green's function for CO_2 is taken directly from Joos et al. (2013):

$$G_{CO2}(t) = a_0 + \sum_{i=1}^{3} a_i e^{t/\tau_i}, \qquad (13)$$

where the parameters are shown in Table 2. The quantity E_{CO2} is the CO_2 emission in $\mathrm{ppm\,yr^{-1}}$ that has been converted from $\mathrm{GtC\,yr^{-1}}$ using the Carbon molecular weight as $E_{CO2}[\mathrm{ppm\,yr^{-1}}] = \gamma\, E_{CO2}[\mathrm{GtC/yr}]$, with $\gamma = 0.46969\,\mathrm{ppm\,GtC^{-1}}$. The emissions for the RCP scenarios are taken from Meinshausen et al. (2011) [1]. The carbon model underestimates CO_2 levels for very high emission scenarios as it does not include saturation of natural CO_2 sinks.

Following Table 8.SM.1 of Myhre et al. (2013) we obtain the changes in radiative forcing compared to preindustrial (in $\mathrm{W\,m^{-2}}$) due to changes in CO_2 as

$$\Delta F_{CO2} = \alpha_{CO2} \ln \frac{C_{CO2}}{C_0}, \qquad (14)$$

where C_0 is the pre-industrial (1750) CO_2 concentration.

We use the same PlaSim ensemble of instantaneous CO_2 doubling runs again to determine a Green's function that relates radiative forcing changes to temperature changes as

$$\Delta T(t) = \int_0^t G_T(\tau)\Delta F(t-\tau)d\tau \qquad (15)$$

where G_T is the data-based function determined from LRT. The total radiative forcing is taken as $\Delta F_{tot} = A\Delta F_{CO2}$. where we introduce a scaling constant A to correct for the high climate sensitivity of the PlaSim model compared to typical CMIP5 models. Based on trial runs attempting to reconstruct mean CMIP5 RCP temperature trajectories with RCP CO_2 emissions we choose $A = 0.6$.

For PlaSim, the Green's function G_T, as determined through LRT, is well approximated by a one-time scale exponential:

$$G_T(t) \approx b_1 e^{-t/\tau_{b1}}, \qquad (16)$$

with $b_1 = 0.25\,\mathrm{K\,W^{-1}\,m^2\,yr^{-1}}$ and $\tau_{b1} = 4.69\,\mathrm{yr}$. We determine a Green's function for the temperature variance in the same way.

---

[1] See the database at http://www.pik-potsdam.de/~mmalte/rcps/

Table 2. Model Parameters. No units are given for dimensionless parameters

$C_{CO2,0}$ (ppm)	278	α_{CO2}	5.35	C_0 (ppm)	278
a_0	0.2173	A	0.6	γ (ppm GtC^{-1})	0.46969
a_1	0.2240	a_2	0.2824	a_3	0.2763
τ_1 (yr)	394.4	τ_2 (yr)	36.54	τ_3 (yr)	4.304

To compute the Point of No Return π_t^{2100} in the carbon-climate model we start from pre-industrial CO_2 concentrations and take the corresponding initial temperature perturbation as $\Delta T = 0$. We then prescribe the RCP emissions scenarios for RCP2.6, RCP4.5, RCP6 and RCP8.5 (that are identical up to the year 2005). At a year $t_b > 2005$ we start reduction of emissions at an exponential rate, i.e. for $t > t_b$ the emissions follow

$$E_{CO2}(t) = E_{CO2}(t_b)\exp\left(-\frac{t - t_b}{\tau_e}\right) \tag{17}$$

where $\tau_e = 25\,\text{yr}$ is the e-folding timescale of the emission reduction that we keep constant. Using the carbon model we compute the instantaneous CO_2 concentrations for each such scenario and use the Green's functions for GMST mean and variance to determine the PDF at year 2100 for each starting year t_b. Assuming Gaussian distributions (as mentioned, this is well satisfied for the original PlaSim ensemble) we can then easily determine the temperature threshold below which 90% of the values fall. The first year for which this threshold is above $2\,\text{K}$ gives π_t^{2100}. Note that the value of t_c (in Fig. 1b) where the CO_2 starts to decrease is determined by the coupled carbon-climate model.

The warming in 2100 predicted by our simple climate model when starting exponential CO_2 emission reduction in a given year is shown in Fig. 7a. The intersections between the RCP curves (solid color) and the dashed line (giving $2\,\text{K}$ warming) provide values of π_t^{2100}. Values do not differ much for the different RCP (4.5, 6.0 and 8.5) scenarios and are before 2030. RCP2.6 does not have a Point of No Return as its emission scenario is sufficient to keep the warming safely below $2\,\text{K}$. The counter-intuitive lowering of the curve for RCP2.6 (also slightly for RCP4.5) is due to very fast emission reductions in these RCP scenarios. So starting emission reduction at later times may lead to lower total emissions (and hence, temperatures). The CO_2 concentration for the four RCP scenarios as computed by the model (solid) and following the exponential mitigation starting from the Point of no Return (dashed) are shown in Fig. 7b. Note how emissions 'still in the pipeline' lead to CO_2 increases even after the reduction is initiated. Note that this approach does not factor in the uncertainty in the carbon model as we do not have a Green's function propagating the carbon uncertainty through the temperature model. Including this would very likely increase the variance in the pdf and move the Point of No Return to an earlier year. On the other hand, the PLASIM variance is quite small, so the 90% threshold is not vastly different from the mean.
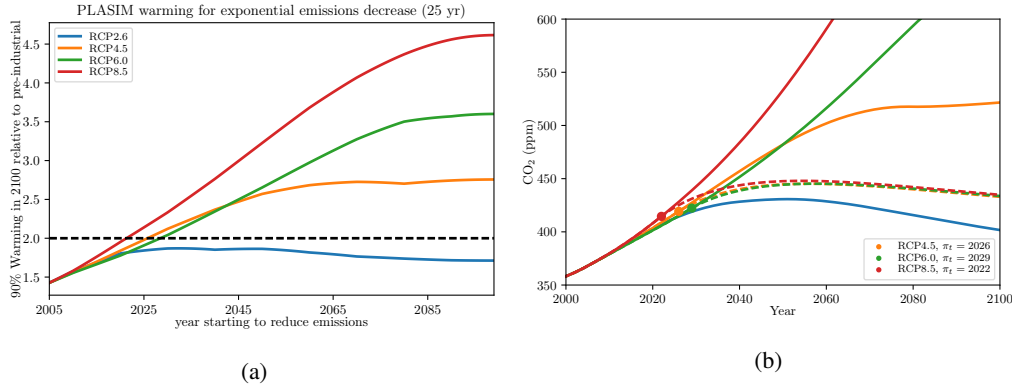
Figure 7. *(a) Warming in 2100 when starting exponential CO_2 emission reduction in a given year. (b) CO_2 concentration for the four RCP scenarios as computed by the model (solid) and following exponential mitigation starting from the Point of no Return (dashed).*

5 Discussion

Pachauri et al. (2014) stated with high confidence that: "Without additional mitigation efforts beyond those in place today, and even with adaptation, warming by the end of the 21st century will lead to high to very high risk of severe, widespread and irreversible impacts globally". If no measures are taken to reduce GHG emissions during this century and neither will there be any new technological developments that can reduce GHGs in the atmosphere, it is likely that the GMST will be 4 °C higher than the preindustrial GMST at the end of the 21st century (Pachauri et al., 2014). Consequently, it is important that anthropogenic emissions are regulated and significantly reduced before widespread and irreversible impacts occur. It would help motivate mitigation to know when it is 'too late'.

In this study we have defined the concept of the Point of No Return (PNR) in climate change more precisely, using stochastic viability theory and a collection of mitigation scenarios. For an energy balance model, as in section 3, the probability density function could be explicitly computed and hence stochastic viability kernels could be determined. The additional advantage of this model is that one can easily construct a bistable regime, so one can investigate the effects of tipping behavior on the PNR. We used this model (where the assumption was made that CO_2 could be controlled directly instead of through emissions), to illustrate of concept of PNR which is based on a tolerance time for which the climate state is non viable. For the RCP scenarios considered, one finds that the PNR is smaller in the bistable than in the monostable regime of this model. The occurrence of possible transitions to warm states in this model indeed cause the PNR to be 'too late' earlier.

The determination of the PNR in the high-dimensional PlaSim climate model, however, shows the key innovation in our approach, i.e. the use of linear response theory (LRT) to estimate the probability density function of the GMST. PlaSim was used to compute another variant of a PNR based on only requiring that the climate state is viable in the year 2100. Hence, the PNR here is the time such that no allowed mitigation scenario can be chosen to keep GMST below a certain threshold

at year 2100 with a specified probability. In the PlaSim results, we used a viability region that was
defined as GMSTs lower than 2°C above the pre-industrial value, but with our methodology, the
PNR can be easily determined for any threshold defining the viable region. The more academic case
where we assume that GHG levels can be controlled directly provides PNR (for RCP4.5, RCP6.0 and
RCP8.5) values around 2050 (section 4.2). However, the more realistic case where the emissions are
controlled (section 4.3) and a carbon model is used, reduces the PNR for these three RCP scenarios
by about 30 years. The reason is that there is a delay between the decrease in GHG gas emissions
and concentrations.

Although our approach provides new insights into the PNR in climate change, we recognize there
is potential to substantial further improvement. First of all, the PlaSim model has a too high climate sensitivity compared to CMIP5 models. Although in the most realistic case (section 4.3), we
somehow compensate for this effect, it would be much better to apply the LRT approach to CMIP5
simulations. Second, in the LRT approach, we assume the GMST distributions to be Gaussian. This
is well justified in PlaSim, as can be verified from the PlaSim simulations, but it may not be the case
for a typical CMIP5 model. Third, for the more realistic case in section 4.3, we do not capture the
uncertainties in the carbon model and hence in the radiative forcing.

A large ensemble such as that available for PlaSim is not available (yet) for any CMIP5 model.
However, we have recently applied the same methodology to two CMIP5 ensembles of models,
i.e. a 34 member ensemble of abrupt CO_2 quadrupling and a 35 member ensemble of smooth 1%
CO_2 increase per year. The CO_2quadrupling ensemble was used to derive the Green's function and
then the 1% CO_2 increase ensemble was used as a check on the resulting response. The probability
density function of GMST increase is close to Gaussian for the 1% CO_2 increase ensemble but
clearly deviates from a Gaussian distribution for the 4x CO_2 forcing ensemble, particularly at later
times. Although the ensemble is relatively small and the models within the ensemble are different
(but many are related), the results for the LRT determined GMST response (Aengenheyster, 2017)
are surprisingly good. This indicates that the methodology has a high potential to be successfully
applied to results of simulations of CMIP5 (and in the future CMIP6) models. The applicability of
LRT to other observables than GMST can in principle be performed but the results may be less
useful (e.g. due to non-Gaussian distributions).

Because PlaSim is highly idealized compared to a typical CMIP5 model one cannot attribute much
importance to the precise PNR values obtained for the PlaSim model as in Fig. 7. However, we think
that our approach is general enough for handling many different political and socio-economical scenarios combined with state-of-the-art climate models when adequate response functions of CMIP5
models have been determined (e.g. using LRT). Hence, it will be possible to make better estimates
of the PNR for the real climate system. We therefore hope that eventually these ideas on the PNR
in climate change will become part of the decision-making process during future discussions about
climate change.

Acknowledgements. This study was supported by the MC-ETN CRITICS project. We thank Valerio Lucarini and Frank Lunkeit (Univ. Hamburg) to provide the PlaSim model data. We thank the reviewers for the critical, excellent and stimulating comments which improved the paper substantially.

References

465   Aengenheyster, M.: The point of no return in climate change has passed!, MSc. thesis, University of Utrecht, p. 22, 2017.

Aubin, J.-P.: Viability theory, Springer Science & Business Media, 2009.

Budyko, M.: Effect of solar radiation variation on climate of Earth, Tellus, 21, 611–619, 1969.

Doyen, L. and De Lara, M.: Stochastic viability and dynamic programming, Systems & Control Letters, 59,
470   629–634, 2010.

Edenhofer, O., Knopf, B., Barker, T., Baumstark, L., Bellevrat, E., Chateau, B., Criqui, P., Isaac, M., Kitous, A., Kypreos, S., et al.: The economics of low stabilization: model comparison of mitigation strategies and costs, The Energy Journal, pp. 11–48, 2010.

Fraedrich, K., Jansen, H., Kirk, E., Luksch, U., and Lunkeit, F.: The Planet Simulator: Towards a user friendly
475   model, Meteorologische Zeitschrift, 14, 299–304, 2005.

Hansen, J., Sato, M., Kharecha, P., Beerling, D., Berner, R., Masson-Delmotte, V., Pagani, M., Raymo, M., Royer, D. L., and Zachos, J. C.: Target atmospheric CO2: Where should humanity aim?, arXiv preprint arXiv:0804.1126, 2008.

Heitzig, J., Kittel, T., Donges, J. F., and Molkenthin, N.: Topology of sustainable management of dynamical sys-
480   tems with desirable states: from defining planetary boundaries to safe operating spaces in the Earth system, Earth System Dynamics, 7, 21–50, 2016.

Hogg, A. M.: Glacial cycles and carbon dioxide: A conceptual model, Geophysical research letters, 35, 2008.

Joos, F., Roth, R., Fuglestvedt, J. S., Peters, G. P., Enting, I. G., von Bloh, W., Brovkin, V., Burke, E. J., Eby, M., Edwards, N. R., Friedrich, T., Frölicher, T. L., Halloran, P. R., Holden, P. B., Jones, C., Kleinen,
485   T., Mackenzie, F. T., Matsumoto, K., Meinshausen, M., Plattner, G.-K., Reisinger, A., Segschneider, J., Shaffer, G., Steinacher, M., Strassmann, K., Tanaka, K., Timmermann, A., and Weaver, A. J.: Carbon dioxide and climate impulse response functions for the computation of greenhouse gas metrics: a multi-model analysis, Atmospheric Chemistry and Physics, 13, 2793–2825, doi:10.5194/acp-13-2793-2013, http://www.atmos-chem-phys.net/13/2793/2013/, 2013.

490   Mann, M. E.: Defining dangerous anthropogenic interference, Proceedings of the National Academy of Sciences, 106, 4065–4066, 2009.

Meinshausen, M., Smith, S. J., Calvin, K., Daniel, J. S., Kainuma, M. L. T., Lamarque, J.-F., Matsumoto, K., Montzka, S. A., Raper, S. C. B., Riahi, K., Thomson, A., Velders, G. J. M., and van Vuuren, D. P.: The RCP greenhouse gas concentrations and their extensions from 1765 to 2300, Climatic Change, 109, 213–241,
495   doi:10.1007/s10584-011-0156-z, http://link.springer.com/10.1007/s10584-011-0156-z, 2011.

Myhre, G., Shindell, D., Bréon, F.-M., Collins, W., Fuglestvedt, J., Huang, J., Koch, D., Lamarque, J.-F., Lee, D., Mendoza, B., Nakajima, T., Robock, A., Stephens, T., Takemura, T., and Zhang, H.: Anthropogenic and Natural Radiative Forcing Supplementary Material, in: Climate Change 2013 - The Physical Science Basis, edited by Change, I. P. o. C., chap. 8, Cambridge University Press, Cambridge, 2013.

500   Pachauri, R. K., Allen, M., Barros, V., Broome, J., Cramer, W., Christ, R., Church, J., Clarke, L., Dahe, Q., Dasgupta, P., et al.: Climate Change 2014: Synthesis Report. Contribution of Working Groups I, II and III to the Fifth Assessment Report of the Intergovernmental Panel on Climate Change, 2014.

Petschel-Held, G., Schellnhuber, H. J., Bruckner, T., Tóth, F. L., and Hasselmann, K.: The Tolerable Windows Approach: Theoretical and Methodological Foundations, Climatic Change, 41, 303–331, 1999.

505 Ragone, F., Lucarini, V., and Lunkeit, F.: A new framework for climate sensitivity and prediction: a modelling perspective, arXiv preprint arXiv:1403.4908, 2014.

Ragone, F., Lucarini, V., and Lunkeit, F.: A new framework for climate sensitivity and prediction: a modelling perspective, Climate Dynamics, 46, 1459–1471, doi:10.1007/s00382-015-2657-3, 2016.

Rogelj, J., Hare, W., Lowe, J., van Vuuren, D. P., Riahi, K., Matthews, B., Hanaoka, T., Jiang, K., and Mein-

510 shausen, M.: Emission pathways consistent with a 2°C global temperature limit, Nature Publishing Group, 1, 413–418, 2011.

Rypdal, K.: Global warming projections derived from an observation-based minimal model, Earth System Dynamics, 7, 51–70, doi:10.5194/esd-7-51-2016, http://www.earth-syst-dynam.net/7/51/2016/, 2016.

Sellers, W. D.: A global climatic model based on the energy balance of the earth-atmosphere system, Journal of

515 Applied Meteorology, 8, 392–400, 1969.

Smith, J. B. and Schneider, S. H.: Assessing dangerous climate change through an update of the Intergovernmental Panel on Climate Change (IPCC)"reasons for concern", in: Proceedings of the National Academy of Sciences, 2009.

Victor, D. G. and Kennel, C. F.: Climate policy: Ditch the 2 C warming goal, Nature, 514, 2014.